Photoconductive terahertz near-field detector with a hybrid nanoantenna array cavity

Oleg Mitrofanov,[1,2,] Igal Brener, [2,3] Ting Shan Luk,[2,3] John L. Reno [2,3]*

[1] University College London, Electronic and Electrical Engineering, London, WC1E 7JE UK

[2] Center for Integrated Technologies, Sandia National Laboratory, Albuquerque, NM 87185, USA

[3] Sandia National Laboratory, Albuquerque, NM 87185, USA

ABSTRACT: Nanoscale structuring of optical materials leads to modification of their properties and can be used for improving efficiencies of photonic devices and for enabling new functionalities. In ultrafast opto-electronic switches for generation and detection of terahertz (THz) radiation, incorporation of nanostructures allows us to overcome inherent limitations of photoconductive materials. We propose and demonstrate a nanostructured photoconductive THz detector for sampling highly localized THz fields, down to the level of $\lambda/150$. The nanostructure that consists of an array of optical nanoantennas and a distributed Bragg reflector, forms a hybrid

cavity, which traps optical gate pulses within the photoconductive layer. The effect of photon trapping is observed as enhanced absorption at a designed wavelength. This optically thin photoconductive THz detector allows us to detect highly confined evanescent THz fields coupled through a deeply sub-wavelength aperture as small as 2 μm (λ/150 at 1 THz). By monolithically integrating the THz detector with apertures ranging from 2 μm to 5 μm we realize higher spatial resolution and higher sensitivity in aperture-type THz near-field microscopy and THz time-domain spectroscopy.

The use of nanostructures for enhancing optical absorption has enabled optically thin semiconductor photonic devices for a wide range of applications, including high-efficiency, low-cost solar cells (1, 2) and photo-detectors based on two-dimensional (2D) atomically thin crystals (3). Nanostructures can also make an impact on development of photoconductive (PC) terahertz (THz) emitters and detectors (4-13). Substantial increase in the conversion efficiency has been achieved in PC THz emitters by coupling the photo-excitation to localized plasmonic modes supported by nanostructured electrodes (5-7). Apart from improving efficiencies, enhancing optical absorption in thin PC layers could enable device concepts deemed impossible until recently. One such device is a PC THz near-field probe for sub-wavelength resolution THz imaging and spectroscopy (12) in which the input aperture is smaller than 1/100 of the wavelength. This probe allows mapping the THz electric field distribution in space and time by optically sampling the THz field that couples through the aperture. Spatial resolution of this near-field probe is defined by the aperture size. Applications of this technique with larger apertures have already demonstrated THz imaging and spectroscopy of fundamental modes in

sub-wavelength size THz resonators (14, 15), and mapping of THz surface waves (16) and transient photocurrents (17). Improving the spatial resolution further however entails detection of THz waves transmitted through a single aperture smaller than ~λ/100, which so far has been impractical.

In previous work it was shown that incorporation of a THz detector near the input aperture in a monolithic probe enhances its sensitivity (18-21). This is because the waves transmitted through the sub-wavelength aperture consist predominantly of evanescent components (22, 23) (described by imaginary k-vectors), which cannot be detected by a far-field detector. However, even the monolithic probes have been impractical for PC THz detectors integrated with apertures smaller than 3 μm (~λ/100 at 1 THz). This is due to the fact that the corresponding THz evanescent field region is smaller than the optical absorption length in commonly used PC materials, such as the low temperature grown GaAs (LT GaAs). THz detectors based on two-dimensional electron gas (2DEG) in GaAs quantum wells and on an electro-optic crystal were also employed to detect THz fields transmitted through sub-wavelength apertures (19, 20). The cryogenically cooled ultrathin 2DEG detector (19) in particular can be highly sensitive to the strongly localized evanescent field and it was demonstrated with apertures as small as 8 μm (19). However this detector lacks the capability of coherent (amplitude and phase) and time-resolved detection, presently possible only with optically-gated THz detectors.

Recent numerical calculations of the evanescent fields near small apertures (12, 20) suggested that monolithic PC THz detectors can enable room-temperature time-resolved THz microscopy with apertures smaller than 3 μm if enhanced optical absorption is realized in optically thin (100-300 nm) PC layers. In general, enhanced light absorption has been achieved using the following design principles: (*i*) light trapping in the absorbing layer by waveguiding (24-30), (*ii*) excitation

of localized plasmonic modes at the interface with the absorbing layer (4-10, 31, 32), and (*iii*) positioning the thin absorbing layer near a metallic plane (e.g. the Salisbury screen) (33-36). In the monolithic PC THz near-field probe, where the optical gate beam and the THz wave are incident on the detector from opposite directions, a metallic plane would block the THz field. Plasmonic electrodes, on the other hand, may result in an increase of the detector's noise current (37). Therefore the most appropriate method to enhance optical absorption for the THz PC detector is to trap the photons in a thin PC region matched in size to the region of localized evanescent THz field.

We propose and demonstrate light trapping in the PC layer using a hybrid optical cavity consisting of a sparse nanoantenna array on one side of the layer and a distributed Bragg reflector (DBR) on the other side. In this structure, the nanoantenna array eliminates the high reflectance at a designed wavelength within the stop band of the DBR almost entirely, and traps the optical gate photons by resonant scattering in the optically thin (280 nm) PC layer, now acting also as a waveguide. The photons therefore remain confined in PC layer until they are absorbed. Enabled by the coupling between the antenna array and the PC layer, this nanostructure provides the possibility for manipulating optical properties of the PC material, enhancing the antenna response within a band substantially narrower than the resonance line-width of individual antennas. The photonic structure allows us to maximize the overlap between the THz evanescent field region of the sub-wavelength aperture and the photo-excitation region as well as to efficiently use the optical gate pulse energy. It enhances responsivity of the sub-wavelength aperture THz near-field probe and allows employing 2 μm input apertures, leading to a higher spatial resolution than previously reported (12).

The structure and the operation principle of the near-field probe are schematically illustrated in Fig. 1. The PC detector consists of a 280 nm thick LT GaAs layer with two metallic electrodes separated by a 2 µm wide gap for collecting the photo-current; a DBR stack made of 4 pairs of AlAs/Al$_{0.2}$Ga$_{0.8}$As layers (thickness of 68 nm and 58.5 nm respectively); and a sparse array of gold nanoantennas isolated electrically from the LT GaAs layer by a thin (15-20 nm) layer of Al$_2$O$_3$ [Fig. 1(b)]. The detector is bonded to a sapphire substrate, which provides optical access to the PC layer. To bring the PC layer as close to the aperture as possible, the DBR stack is etched away everywhere except for a square shape area centered between the metallic electrodes. A 300 nm thick metallic screen is deposited on the probe surface around the 466 nm thick DBR stack. As a result, a dielectric filled aperture is formed in the screen. To prevent short-circuit current in the THz detector, we isolate the metallic screen electrically from the PC layer using a 30 nm thick Al$_2$O$_3$ film.

Detection of THz radiation coupled through the aperture is realized in the same manner as with PC THz receivers used in THz time-domain spectroscopy systems. A schematic diagram of the system is shown in Fig. 1(c). THz pulses are generated in a ZnTe crystal by the process of optical rectification using 100 fs near-infrared (NIR) pulses from a Ti:sapphire laser (λ_o=820 nm). The THz beam is focused on the aperture area of the probe at normal incidence using a Si lens attached to the ZnTe crystal. The beam size is approximately 500 µm in diameter. The THz field that couples through the aperture induces an oscillating THz electric field in the LT GaAs region [Fig. 1(a)]. To detect that field, photo-conductivity in the field region is switched on by a NIR gate pulse from the same laser, focused on the PC region through the sapphire substrate using an aspheric lens with NA=0.5. The photo-generated charge carriers drift in the THz field and produce photocurrent between the electrodes proportional to the instantaneous THz field. The

THz pulse waveform is then sampled by varying the arrival time of the gate NIR pulse with respect to the THz pulse using a time-delay stage [Fig. 1(c)].

Within the photonic structure, the gate pulse photons first encounter the array of sparse nanoantennas, which scatter the incident photons (38-41). The fundamental antenna resonance (along the antenna length) is designed to match the optical excitation wavelength $\lambda_\square$. Photons scattered into angles larger than the critical angle become trapped in the high-index LT GaAs layer due to total internal reflection [Fig. 1(d)], whereas photons that experience small-angle or no scattering are reflected by the DBR stack [Fig. 1(d)]. To increase the reflection coefficient of the DBR, the LT GaAs layer thickness itself is chosen to be a multiple of ¼ of the optical excitation wavelength in GaAs, $L = (1+ ¼) \lambda_\square/n_{GaAs} = 280$ nm.
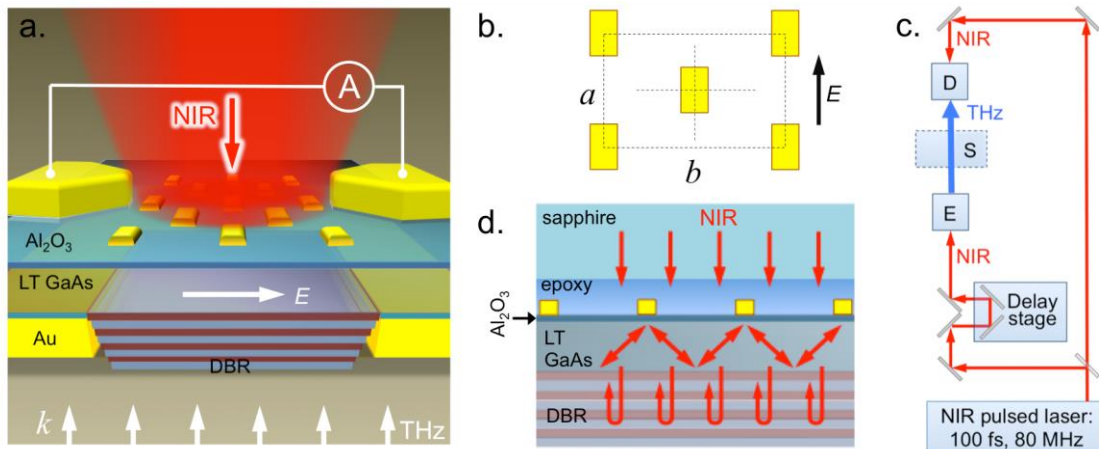

Figure 1. a) Schematic diagram of the PC THz near-field probe. White arrows indicate the wavevector of the incident THz wave (k) and the electric field (E) induced in the photoconductive region. The red arrow indicates the optical gating pulse (NIR). b) Unit cell of the antenna array: a=250 nm, b=400 nm. The black arrow shows the optical excitation polarization. c) Schematic diagram of the THz near-field microscopy system with the monolithic

PC detector probe: the ZnTe crystal (E) is excited by NIR pulses from the Ti:sapphire laser; the generated THz pulses are directed to the near-field probe (D), where the THz field is sampled by gating the PC THz detector with NIR pulses from the same laser. A sample (S) can be placed between the emitter and the detector for THz near-field imaging and spectroscopy. d) Schematic cross-section diagram of the photonic structure and its operation principle. The NIR gate pulse (red arrows) is trapped in the LT GaAs layer after scattering on the nanoantenna array shown schematically as yellow squares.

We design the nanoantenna array to have a plasmonic resonance at the laser excitation wavelength using a commercial finite difference time-domain (FDTD) solver (42). The dimensions of each antenna are chosen to be 100 nm x 66 nm x 65 nm (*length* x *width* x *height*) for compatibility with electron beam lithography. When arranged in the configuration shown in Fig. 1(b) and embedded into the dielectric environment shown in Fig. 1(d), the antenna array without the DBR stack exhibits a broad resonance at 800 nm according to the simulations (see Supplementary Information).

First we analyze the optical properties of the photonic structure to evaluate whether it efficiently absorbs NIR photons. The structure without the array shows the characteristic stop-band of a DBR mirror with the center wavelength around 810 nm [Fig. 2(a, b), black lines]. The LT GaAs layer in this case acts as the first high-index layer of the stack and it absorbs only ~35% of the incident photons. Combining the DBR with the antenna array however changes the optical properties drastically: the reflectivity spectrum develops a significant drop (from ~60% to below 5%) within the stop band, similar to that of a dielectric high-index planar cavity.

Remarkably, the transmission coefficient at the wavelength of the dip remains practically unchanged.

Experimental transmission and reflection are characterized using a linearly polarized, focused broadband optical beam with NA=0.5, similar to that of the optical gate beam. The experimental spectra closely match the simulated spectra. For the antennas oriented parallel to the beam polarization, the reflection coefficient decreases to 5% at 820 nm, whereas the transmission coefficient remains less than 5% at 800 nm rising only to 10% at 830 nm. Based on the experimental spectra, 80-85% of the NIR gate beam with λ_o in the range of 800-830 nm can be absorbed in the photonic structure despite the fact the LT GaAs layer is thinner than ¼ of the absorption length. In contrast to the structure without the antenna array, the majority of laser photons are converted into charge carriers in the PC layer. For the probing beam polarized orthogonally to the long axis of the antenna, we find the dip in reflectivity disappear and the transmission spectrum in Fig. 2a become similar to the spectrum without the antennas.
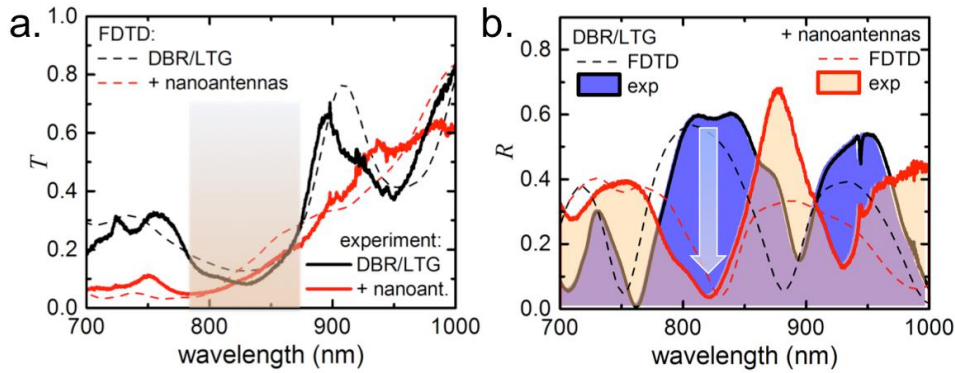

Figure 2. Transmission (a) and reflection (b) spectra of the DBR with the LT GaAs layer (DBR/LTG) with (red) and without (black) the antenna array. Experimental and simulated

spectra are shown by the solid and dashed lines respectively. The shaded area in (a) marks the stop band of the DBR stack; the arrow in (b) indicates the reflectivity drop.

To understand the origin of this reflectivity dip, we consider the effect of nanoantennas on the field distribution in the LT GaAs layer. The array imposes periodic variation of the optical field in the transverse direction. Therefore the momentum of photons in the LT GaAs layer has an in-plane component $k_y = 2\pi/p$, where $p=b=400$ nm is the array periodicity. The LT GaAs layer therefore can acts as a planar waveguide or a cavity with modes described by the total k-vector condition expressed as:

$$k_m = \frac{\sqrt{k_y^2 + \dfrac{p^2 m^2}{L^2}}}{n_{GaAs}},$$ (1)

where m is an integer (43). The corresponding wavelength for $m=2$, $\lambda_2 = 826$ nm, matches the wavelength of the reflectivity dip in Fig. 2(c). The fact that the spectral width of the reflectivity dip is 50 nm, significantly narrower than the width of the antenna resonance (~200 nm, see Supplementary Information), confirms that the reflectivity dip corresponds to the hybrid cavity mode, rather than to the pure antenna resonance.

The strong decrease of reflectivity and the lack of a Fabry-Perot peak in the transmission spectrum indicate efficient scattering of the incident photons into the LT GaAs layer. These photons are guided by total internal reflection on one side of the layer and by the DBR stack on the other side until they excite electron-hole pairs. The nanoantenna array therefore transforms the LT GaAs layer into a cavity that traps the incident photons.

The enhancement of optical absorption within the LT GaAs layer is verified by comparing the photocurrent response of identical THz detectors with and without the array [Fig. 3(a)]

incorporated into the PC region between the electrodes [Fig. 3(b)]. An over 50% increase in the photocurrent is observed for the detectors with nanoantennas. The peak photocurrent, corresponding to the maximum temporal overlap of the THz pulse and the optical gate pulse, reaches ~ 500 pA for the gate average power of 5 mW. The photocurrent increase is consistent with the experimentally measured reflectivity and transmission spectra. We emphasize that dark resistance of these detectors remains in the region of 2-3 GΩ after introducing the nanoantennas. The increase in detection sensitivity therefore is achieved without an increase in detector noise.
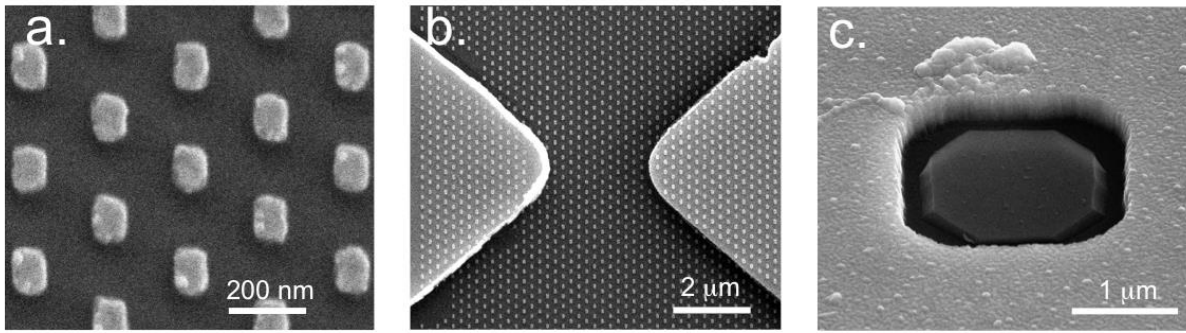

Figure 3. Scanning electron micrographs of the gold antenna array (a); the active region of the THz detector showing two metallic electrodes and the nanoantenna array in the PC gap (b); and a 2 μm square input aperture in the gold screen of the near-field THz probe (c).

The realization of enhanced optical absorption in a thin PC layer allows us to capture the evanescent fields for apertures as small as 2 μm. Waveforms of THz pulses transmitted through square apertures of 2, 3 and 5 μm and their corresponding Fourier spectra are shown in Fig. 4(a, b). A distinctive THz pulse waveform is detected for all the apertures. The waveform shape agrees with the temporal derivative of the incident pulse waveform (44). For the 5 μm aperture (λ/60), the detected field amplitude is reduced only by a factor of ~20, compared to the

amplitude of the incident field. This is a significant improvement compared to the factor of ~1000 found in a monolithic probe employing a 1 μm thick PC layer (without the photonic structure) integrated at 4 μm away from the aperture plane (18).

For the nanostructured probe, the detected electric field amplitude (averaged in the 1.0-1.5 THz band) follows approximately the $a^{2.6}$ dependence for aperture sizes between 5 μm to 2 μm [Fig. 4(b), inset], in agreement with electromagnetic FDTD simulations (12). Probes with a 2 μm input aperture detect the THz pulse waveform with a practical signal to noise ratio. To our knowledge, this is the first demonstration that THz pulses coupled through a 2 μm square aperture (λ/150 at 1 THz) can be detected and used for local THz spectroscopy analysis.

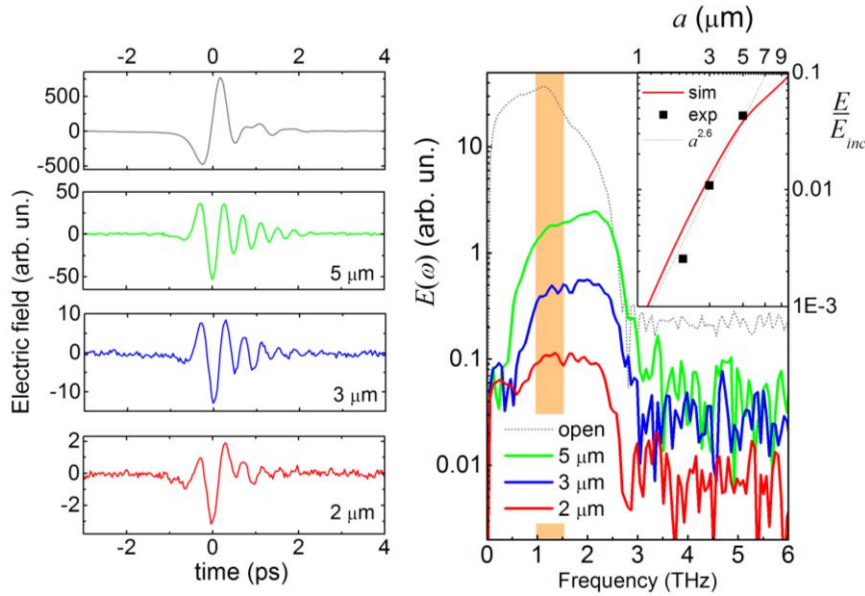**Figure 4.** (a) Time-domain waveforms of THz pulses transmitted through the 5, 3 and 2 μm square apertures compared to the incident pulse waveform (top). (b) Fourier transform spectra of the pulses in (a); the inset shows the detected field amplitude as a function of the aperture size; the amplitude is averaged over the 1.0-1.5 THz band (shaded area) and normalized to the corresponding amplitude of the incident pulse.

In conclusion, we show that integrating a nanoantenna array and a distributed Bragg reflector with an optically thin PC THz detector enhances optical absorption and results in an increase in detection sensitivity without noise penalty for sub-wavelength aperture THz probes. The nanostructured THz PC detector allows us to sense the highly confined THz fields coupled through single apertures as small 2 μm (λ/150 at 1THz). The nanostructure provides two critical functions: first of all, it localizes the optical gate pulses uniformly within the evanescent field region of the aperture; secondly, it efficiently converts the gate pulse photons into photo-carriers in an optically thin LT GaAs layer. The concept of THz near-field probe with an optically thin nanostructured PC THz detector opens doors for improving spatial resolution and sensitivity in sub-wavelength aperture THz near-field microscopy. In this work we demonstrate that 2 μm aperture near-field probes (λ/150 at 1 THz) that can be employed with full THz time-domain spectroscopy capabilities.

Methods. The AlAs/$Al_{0.2}Ga_{0.8}$As DBR stack and the LT GaAs layer are grown by molecular beam epitaxy (wafer number: VB0656) on a semi-insulating GaAs substrate. The substrate temperature is lowered to 250 C during the GaAs layer growth. The samples are subsequently annealed at 600 C for 40 sec. The metallic electrodes are defined lithographically directly on the surface of the annealed samples. The 15-20 nm thick layer of Al_2O_3 is deposited over the whole device using electron beam physical vapor deposition. The nano-antenna array is fabricated by electron beam lithography. Individual THz detectors are cleaved from the wafer and bonded to a 500 μm thick sapphire plate with a transparent non-conductive epoxy (Epotek 353ND). The GaAs substrate is removed using lapping and chemical etching. The exposed DBR stack is then etched away everywhere except for a square shape area centered between the metallic electrodes. The insulating Al_2O_3 layer and the 300 nm thick gold screen are deposited instead of the etched

DBR layers using electron beam physical vapor deposition. The buried detector electrodes are exposed using chemical etching in an area of the device 5 mm away from the aperture location.

The THz detectors are optically gated by 100 fs pulses from the Ti:sapphire laser with average power of 5 mW focused to an ~2-3 μm spot. The photocurrent from the detector is measured by a current pre-amplifier (DL Instruments) and a lock-in amplifier (Stanford Research Systems, SR830). The typical peak magnitude of the photo-current in the THz detector with nanoantennas is ~500 pA for the 5 mW optical excitation power (See Fig. 4). Typical variation in detector responsivity (peak photocurrent) for devices in the same fabrication batch is ±10%. No degradation in performance of THz detectors with nanoantennas under the 5 mW optical excitation with typical currents of ~ 500 pA have been observed during continuous operation of each detector for 2-3 hours/day. Furthermore, no degradation was observed due to prolonged storage of the devices over 3-4 months.

Supporting Information.

Supplementary figures showing the resonant response of the nanoantenna array. This material is available free of charge via the Internet at http://pubs.acs.org."

Corresponding Author

* e-mail address: o.mitrofanov@ucl.ac.uk

Author Contributions

The manuscript was written through contributions of all authors. All authors have given approval to the final version of the manuscript.

REFERENCES

(1) Atwater, H. A.; Polman, A. Plasmonics for improved photovoltaic devices. *Nat. Materials* **2010,** 9(3), 205-213.

(2) Kim, S. J.; Thomann, I.; Park, J.; Kang, J.-H.; Vasudev, A. P.; Brongersma, M. L. Light trapping for solar fuel generation with Mie resonances. *Nano Lett.* **2014,** 14(3), 1446-1452.

(3) Lei, S.; Wen, F.; Ge, L.; Najmaei, S.; George, A.; Gong, Y.; Gao, W.; Jin, Z.; Li, B.; Lou, J.; Kono, J,; Vajtai, R.; Ajayan, P.; Halas N. J. An atomically layered InSe avalanche photodetector. *Nano Lett.* **2015,** 15, 3048-3055.

(4) Jarrahi, M. Advanced Photoconductive Terahertz Optoelectronics Based on Nano-Antennas and Nano-Plasmonic Light Concentrators. *Terahertz Science and Technology, IEEE Trans.* **2015,** 5(3), 391-397.

(5) Heshmat, B.; Pahlevaninezhad, H.; Pang, Y.; Masnadi-Shirazi, M.; Lewis, R. B.; Tiedje, T.; Gordon, R.; Darcie, T. E. Nanoplasmonic terahertz photoconductive switch on GaAs. *Nano Lett.* **2012,** 12, 6255-6259.

(6) Berry, C. W.; Wang, N.; Hashemi, M. R.; Unlu, M.; Jarrahi, M. Significant performance enhancement in photoconductive terahertz optoelectronics by incorporating plasmonic contact electrodes. *Nature Communications* **2013,** 4, 1622.

(7) Tanoto, H.; Teng, J. H.; Wu, Q. Y.; Sun, M.; Chen, Z. N.; Maier, S. A.; Wang, B.; Chum, C. C.; Si, G. Y.; Danner, A. J.; Chua, S. J. Nano-antenna in a photoconductive photomixer for highly efficient continuous wave terahertz emission. *Scientific Reports* **2013,** 3, 2824.

(8) Berry, C. W.; Hashemi, M. R.; Jarrahi, M. Generation of high power pulsed terahertz radiation using a plasmonic photoconductive emitter array with logarithmic spiral antennas. *Appl. Phys. Lett.* **2014,** 104(8), 081122.

(9) Jooshesh, A.; Smith, L.; Masnadi-Shirazi, M.; Bahrami-Yekta, V.; Tiedje, T.; Darcie, T. E.; Gordon, R. Nanoplasmonics enhanced terahertz sources. *Optics Express* **2014,** 22(23), 27992-28001.

(10) Jafarlou, S.; Neshat, M.; Safavi-Naeini, S. A hybrid analysis method for plasmonic enhanced terahertz photomixer sources. *Optics Express* **2013,** 21(9), 11115-11124.

(11) Peytavit, E.; Lepilliet, S.; Hindle, F.; Coinon, C.; Akalin, T.; Ducournau, G.; Mouret, G.; Lampin, J.-F. Milliwatt-level output power in the sub-terahertz range generated by photomixing in a GaAs photoconductor. *Appl. Phys. Lett.* **2011,** 99, 223508.

(12) Macfaden, A. J.; Reno, J. L.; Brener, I.; Mitrofanov, O. 3 μm aperture probes for near-field terahertz transmission microscopy. *Appl. Phys. Lett.* **2014,** 104, 011110.

(13) Ramanandan, G. K. P.; Adam, A. J. L.; Planken, P. C. M. Enhanced terahertz emission from Schottky junctions using plasmonic nanostructures. ACS Photonics **2014,** 1, 1165-1172.

(14) Mitrofanov, O.; Dominec, F.; Kuzel, P.; Reno, J. L.; Brener, I.; Chung, U.-C.; Elissalde, C.; Maglione, M.; Mounaix, P. Near-field probing of Mie resonances in single TiO_2 microspheres at terahertz frequencies. *Optics Express* **2014,** 22, 23034-23042.

(15) Khromova, I.; Navarro-Cia, M.; Brener, I.; Reno, J. L.; Ponomarev, A.; Mitrofanov, O. Dipolar resonances in conductive carbon micro-fibers probed by near-field terahertz spectroscopy. *Appl. Phys. Lett.* **2015,** 107, 021102.

(16) Mueckstein, R.; Mitrofanov. O. Imaging of terahertz surface plasmon waves excited on a gold surface by a focused beam. *Optics Express* **2011,** 19, 3212-3217.

(17) Mueckstein, R.; Natrella, M.; Hatem, O.; Freeman, J. R.; Graham, C. S.; Renaud, C. C.; Seeds, A. J.; Linfield, E. H.; Davies, A. G.; Cannard, P. J.; Robertson, M. J.; Moodie, D. G.; Mitrofanov, O. Near-field analysis of terahertz pulse generation from photo-excited charge density gradients. *Terahertz Science and Technology, IEEE Trans.* **2015,** 5(2), 260-267.

(18) Mitrofanov, O.; Lee, M.; Hsu, J. W. P., Pfeiffer, L. N.; West, K. W.; Wynn, J. D.; Federici, J. F. Terahertz pulse propagation through small apertures. *Appl. Phys. Lett.* **2001,** 79, 907-909.

(19) Kawano Y.; Ishibashi, K. An on-chip near-field terahertz probe and detector. *Nat. Photonics* **2008,** 2, 618-621.

(20) Knab, J. R.; Adam, A. J. L.; Shaner, E.; Starmans, H. J. A. J.; Planken, P. C. M. Terahertz near-field spectroscopy of filled subwavelength sized apertures in thin metal films. *Optics Express* **2013,** 21(1), 1101-1112.

(21) Misra, M.; Pan, Y.; Williams, C. R.; Maier, S. A.; Andrews, S. R. Characterization of a hollow core fibre-coupled near field terahertz probe. *J. Appl. Phys.* **2013,** 113, 193104.

(22) Bethe, H. Theory of diffraction by small holes. *Phys. Rev.* **1944,** 66, 163.

(23) Bouwkamp, C. On Bethe's theory of diffraction by small holes. *J. Philips Res. Rep.* **1950,** 5, 321-332.

(24) Stuart, H. R.; Hall, D. G. Absorption enhancement in silicon-on-insulator waveguides using metal island films. *Appl. Phys. Lett.* **1996,** 69(16), 2327-2329.

(25) Yablonovitch E.; Cody, G. D. Intensity enhancement in textured optical sheets for solar cells. *IEEE Trans. Electron Devices* **1982,** 29(2), 300-305.

(26) Campbell P.; Green, M. A. Light trapping properties of pyramidally textured surfaces. *J. Appl. Phys.* **1987,** 62(1), 243-249.

(27) Panoiu, N. C.; Osgood, R. M. Enhanced optical absorption for photovoltaics via excitation of waveguide and plasmon-polariton modes. *Opt. Lett.* **2008,** 32(19), 2825-2827.

(28) Catchpole, K. R.; Polman, A. Design principles for particle plasmon enhanced solar cells. *Appl. Phys. Lett.* **2008,** 93, 191113.

(29) Briscoe J. L.; Cho, S.-Y. Hybridised extraordinary optical transmission in plasmonic cavity. *Electron. Lett.* **2014,** 50(24), 1860-1862.

(30) Vasudev, A. P.; Schuller, J. A.; Brongersma, M. L. Nanophotonic light trapping with patterned transparent conductive oxides. *Optics Express* **2012,** 20(S3), A385-A394.

(31) Piper, J.R.; Fan S. Total absorption in a graphene monolayer in the optical regime by critical coupling with a photonic crystal guided resonance. *ACS Photonics* **2014,** 1, 347-353.

(32) Min, C.; Li, J.; Veronis, G.; Lee, J.-Y.; Fan, S.; Peumans, P. Enhancement of optical absorption in thin-film organic solar cells through the excitation of plasmonic modes in metallic gratings. *Appl. Phys. Lett.* **2010,** 96, 133302.

(33) Fante, R. L.; Mccormack, M. T. Reflection properties of the Salisbury screen. *Antennas and Propagation, IEEE Trans.* **1988,** 36(10), 1443-1454.

(34) Thareja, V.; Kang, J.-H.; Yuan, H.; Milaninia, K. M.; Hwang, H. Y.; Cui, Y.; Kik, P. G.; Brongersma, M. L. Electrically tunable coherent optical absorption in graphene with ion gel. *Nano Lett.* **2015,** 15(3), 1570-1576.

(35) Kats, M. A.; Blanchard, R.; Genevet, P.; Capasso, F. Nanometre optical coatings based on strong interference effects in highly absorbing media. *Nature Materials* **2013,** 12, 20-24.

(36) Park, J.; Kang, J. H.; Vasudev, A. P.; Schoen, D. T.; Kim, H.; Hasman, E.; Brongersma, M. L. Omnidirectional Near-Unity Absorption in an Ultrathin Planar Semiconductor Layer on a Metal Substrate. *ACS Photonics*, **2014,** 1(9), 812-821.

(37) Wang, N.; Jarrahi, M. Noise analysis of photoconductive terahertz detectors. *J Infrared Milli Terahz Waves* **2014,** 34, 519-528.

(38) Rosenblatt, D.; Sharon, A.; Friesem, A. Resonant grating waveguide structures. *IEEE J. Quantum Electron.* **1997,** 33, 2038-2059.

(39) Fevrier, M.; Gogol, P.; Aassime, A.; Mégy, R.; Delacour, C.; Chelnokov, A.; Apuzzo, A.; Blaize, S.; Lourtioz, J.-M.; Dagens, B. Giant coupling effect between metal nanoparticle chain and optical waveguide. *Nano Lett.* **2012,** 12, 1032-1037.

(40) Arango, F. B.; Kwadrin, A.; Koenderink, A. F. Plasmonic antennas hybridized with dielectric waveguides. *ACS Nano* **2012,** 6(11), 10156-10167.

(41) Schwarz, I.; Harats, M.G.; Livneh, N.; Yochelis, S.; Strauss, A.; Zimran, A.; Banin, U.; Paltiel, Y.; Rapaport, R. Theory and experiments of Bragg cavity modes in passive and active metallic nanoslit array devices. *J. of the Optical Society of Am. B* **2012,** 29(2), A127-A137.

(42) See http://www.lumerical.com/tcad-products/fdtd/ for Lumerical Solutions, Inc., Lumerical FDTD Solutions.

(43) Novotny, L.; Hecht, B. 'Principles of Nano-Optics,' *Cambridge* 2012.

(44) Mitrofanov, O.; Pfeiffer, L. N.; West, K. W. Generation of low-frequency components due to phase-amplitude modulation of subcycle far-infrared pulses in near-field diffraction. *Appl. Phys. Lett.* **2002,** 81, 1579-1581.